Switched-Battery Boost-Multilevel Inverter with GA Optimized SHEPWM for Standalone Application

Sze Sing Lee, *Member, IEEE*, Bing Chu, Nik Rumzi Nik Idris, *Senior Member, IEEE*, Hui Hwang Goh, *Senior Member, IEEE*, and Yeh En Heng

***Abstract*—This paper presents a boost-multilevel inverter design with integrated battery energy storage system for standalone application. The inverter consists of modular switched-battery cells and a full-bridge. It is multifunctional and has two modes of operation: 1) the charging mode, which charges the battery bank and 2) the inverter mode, which supplies ac power to the load. This inverter topology requires significantly less power switches compared to conventional topology such as cascaded H-bridge multilevel inverter, leading to reduced size/cost and improved reliability. To selectively eliminate low-order harmonics and control the desired fundamental component, nonlinear system equations are represented in fitness function through the manipulation of modulation index and the genetic algorithm (GA) is employed to find the optimum switching angles. A seven-level inverter prototype is implemented and experimental results are provided to verify the feasibility of the proposed inverter design.**

***Index Terms*—Boost-multilevel inverter, genetic algorithm (GA), photovoltaic (PV), selective harmonic elimination (SHE).**

I. Introduction

THE URGENT need to mitigate climate change requires extensive use of energy from renewable resources such as solar, wind, and hydro to reduce the greenhouse gas emissions. Due to the rapid shift from conventional nonrenewable energy source to renewable energy (RE) source, application of power electronics in power distributed generation (DG) industry is becoming a fast evolving technology [1]. Efficient power generation from RE source is highly dependent on the efficiency of the power electronics converter [2]. Extensive research has been done in integrating RE into power grid system. However, there are still a plethora of rural areas in developing countries, which are not accessible to any power grid system [3]. In this occasion, standalone RE system becomes the sole solution. An efficient, reliable power inverter with high performance controller is thus the key to the success of RE integration for such situations where the inverter operates as power supply with mandatory energy storage system [4].

In recent years, multilevel inverters have been receiving wide attention and becoming hot topologies for RE applications [5], [6]. Multilevel inverters can be classified into three types that are flying-capacitor, diode-clamp, and cascaded H-bridge multilevel inverter [7], [8]. Flying capacitor multilevel inverter has several drawbacks: it requires large number of storage electrolytic capacitors; the inverter control can be very complicated; and the switching frequency and switching loss are high [9]. The use of diode-clamp multilevel inverter in photovoltaic (PV) systems has been presented in [10]–[12]. This topology has the problem of unbalance capacitor voltage. Cascaded H-bridge multilevel inverter is among the most popular inverter topology in standalone PV systems [13]–[18]. Fig. 1(a) shows the standalone renewable systems using cascaded H-bridge multilevel inverter. Full-bridge inverters are connected in series with their output voltages are total up and hence, it has voltage boosting capability. However, this inverter topology requires separate dc source for each full-bridge inverter. In order to isolate the input of each full-bridge inverter, all batteries are charged by separate renewable resources (e.g., PV modules) through independent charge controller as depicted in Fig. 1(a). This makes it not easy to use for many standalone applications where only single dc source is available. In addition, this system consists of high number of components and hence, is very costly and bulky.

To make use of cascaded H-bridge multilevel inverter with only single input dc source, multiple isolated dc–dc converters can be used to artificially create multiple isolated dc voltages for each full-bridge [19]. In [20], full-bridges are connected in parallel sharing single dc source with the output of each bridge is isolated by using separate transformers. The secondary of transformers are cascaded to produce multilevel

Manuscript received June 18, 2015; revised September 29, 2015; accepted October 31, 2015. Date of publication December 8, 2015; date of current version March 8, 2016.

S. S. Lee is with the EEE Research Group, School of Electronics and Computer Science (ECS), Faculty of Physical Sciences and Engineering, University of Southampton, Southampton, SO17 1BJ, U.K., and also with the University of Southampton Malaysia Campus (USMC), Johor Bahru 79200, Malaysia (e-mail: ss.lee@soton.ac.uk).

B. Chu is with the School of Electronics and Computer Science (ECS), Faculty of Physical Sciences and Engineering, University of Southampton, Southampton, SO17 1BJ, U.K. (e-mail: B.Chu@soton.ac.uk).

N. R. N. Idris is with the Faculty of Electrical Engineering, Universiti Teknologi Malaysia (UTM), Johor Bahru 81310, Malaysia (e-mail: nikrumzi@fke.utm.my).

H. H. Goh is with the Department of Electrical Power, Faculty of Electrical and Electronic Engineering, Universiti Tun Hussein Onn Malaysia (UTHM), Batu Pahat 86400, Malaysia (e-mail: hhgoh@uthm.edu.my).

Y. E. Heng is with the University of Southampton Malaysia Campus (USMC), Johor Bahru 79200, Malaysia (e-mail: hengyehen@gmail.com).

Color versions of one or more of the figures in this paper are available online at http://ieeexplore.ieee.org.

Digital Object Identifier 10.1109/TIE.2015.2506626

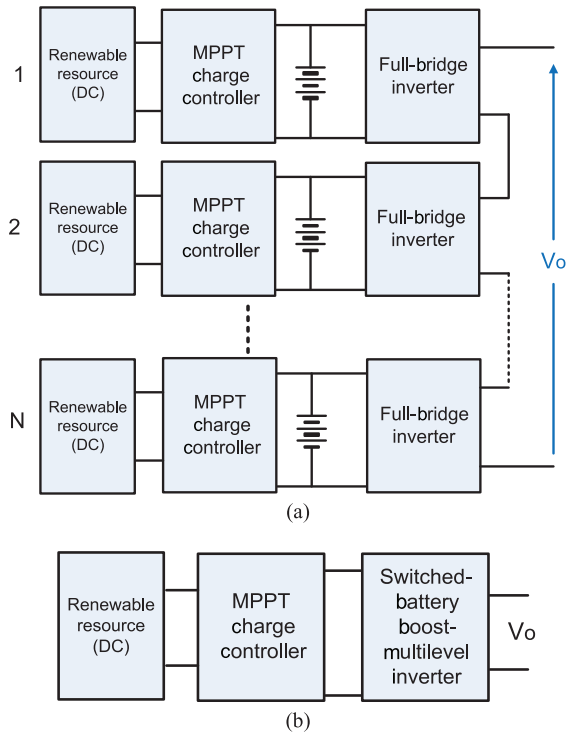

Fig. 1. Configuration of standalone system using (a) conventional cascaded H-bridge multilevel inverter and (b) switched-battery boost-multilevel inverter.

ac voltage. Eliminating multiple dc sources in a cascaded H-bridge multilevel inverter is feasible but comes with a price that extra components need to be added, e.g., dc–dc converters or transformer, which again increases the size and cost. Efforts have also been made to reduce the power switch number in multilevel inverters by proposing alternative topologies [21]. A hybrid topology is proposed in [22] for standalone PV system. Although the number of power switches is reduced significantly, this topology, however, still requires four isolated dc sources. Separate PV string for each dc source is mandatory, which requires multiple maximum power point tracking (MPPT) charge controllers and dc–dc converters. Similarly, multilevel dc-link inverter topology presented in [23] demonstrates the possibility of switch number reduction, however, with a tradeoff of additional isolation transformers and dc–dc converters.

Inspired by the above work, this paper proposes a novel compact multifunctional inverter topology, which integrates battery bank to adapt for standalone application. It can operate in either charging mode or inverter mode. The proposed system is shown in Fig. 1(b). Compared to the conventional cascaded H-bridge multilevel inverter, significantly less number of switches are required, a single renewable resource (e.g., PV string) can be used and only one MPPT charge controller is needed. This inverter is controlled by selective harmonics elimination pulse width modulation (SHEPWM) with genetic algorithm (GA) optimization. This paper is organized as follows. Section II discusses the switched-battery boost-multilevel inverter, Section III elaborates the SHEPWM with GA optimization, Section IV discusses simulation results, Section V describes the hardware implementation, Section VI presents the experimental results, and finally Section VII gives the conclusion.

II. Switched-Battery Boost-Multilevel Inverter

Fig. 2 shows the circuit diagram of one phase-leg of the proposed switched-battery boost-multilevel inverter for standalone application. This topology comprises switched-battery circuit and full-bridge. The switched-battery circuit is a modular network formed by cascading N number of cells. Each cell consists of two power MOSFETs, an SPST relay and a battery as shown in Fig. 3. The battery bank for energy storage system is integrated into the topology and hence, it can be operating in two modes: 1) battery charging mode and 2) inversion mode.

To operate the inverter in charging mode, the SPDT relay is switched to MPPT charge controller and all SPST relays are closed. At the same time, all the topmost power MOSFET of the switched-battery cells $(S_{11}, S_{21}, \ldots, S_{N1})$ are ON while the remaining power MOSFETSs are left in OFF state. Energy generated by renewable resource (e.g., PV module) will be stored in the parallel connected batteries, as depicted in Fig. 4. The conducting power MOSFETs experience low conduction loss due to the low resistivity as they are working in synchronous rectification mode.

The equivalent circuit for inverter mode is shown in Fig. 5. In this mode, the MPPT charge controller is disconnected from the inverter circuit and all SPST relays are OFF. By turning on the bottom-most power MOSFETs $(S_{12}, S_{22}, \ldots, S_{N2})$ of switched-battery cells, the batteries are connected in series. In contrast, turning ON the topmost power MOSFETs isolates the batteries. Power MOSFETs at the topmost level and bottommost level of the switched-battery cells are controlled in complementary sequence as given in Table I. With N switched-battery cells, an N step staircase dc voltage can be produced as the one shown in Fig. 6(a). The magnitude of each voltage step depends on the battery voltage and the maximum voltage equal to NV_{BAT}.

The staircase dc-link voltage can be manipulated to produce multilevel ac voltage by using a full-bridge that alternates the polarity [23]. The number of ac voltage levels N_{Vo} of the switched-battery boost-multilevel inverter is given by

$$N_{\mathrm{Vo}} = 2N + 1 \tag{1}$$

where N is the number of switched-battery cell.

The number of power MOSFET N_{MOS} required is equal to twice the number of switched-battery cell with additional four units for full-bridge inverter. It can be written as

$$N_{\mathrm{MOS}} = 2N + 4 = N_{\mathrm{Vo}} + 3. \tag{2}$$

Therefore, this topology has higher power MOSFET utilization factor as compared to the conventional cascaded H-bridge multilevel inverter. Fig. 7 shows the comparison of the required power MOSFETs. It can be seen that as the number of voltage level increases, the switched-battery boost-multilevel inverter shows significant reduction in number of power MOSFETs. In addition, the inverter possesses integrated energy storage system, which allows it to operate in both charging mode and

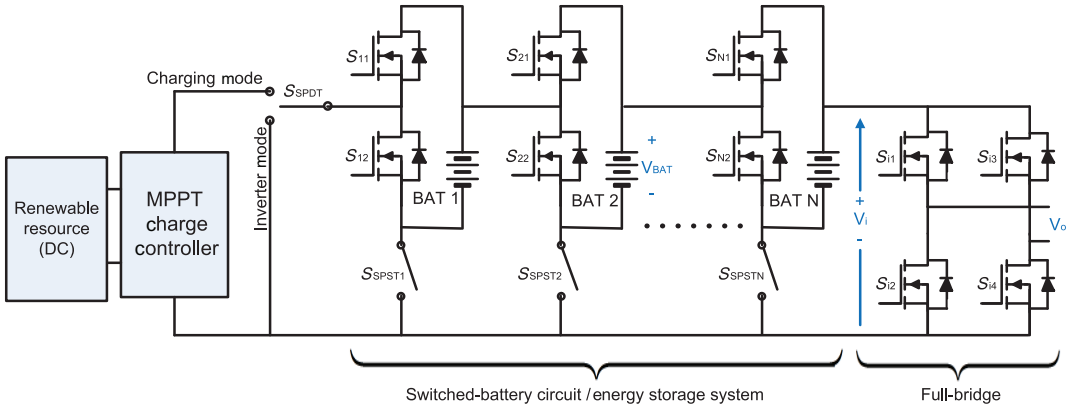

Fig. 2. Circuit diagram of one phase-leg of the proposed switched-battery boost-multilevel inverter for standalone application.

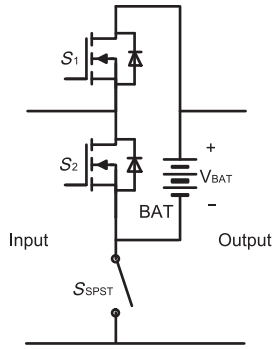

Fig. 3. Switched-battery cell.

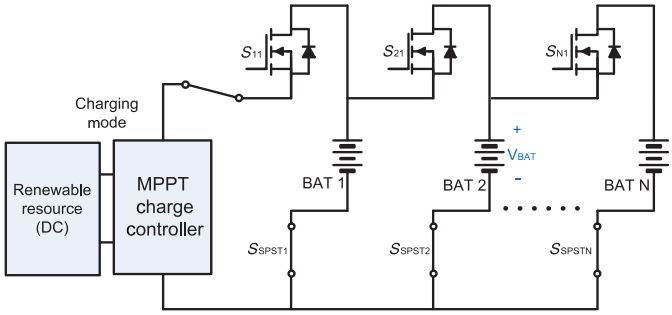

Fig. 4. Equivalent circuit during charging mode.

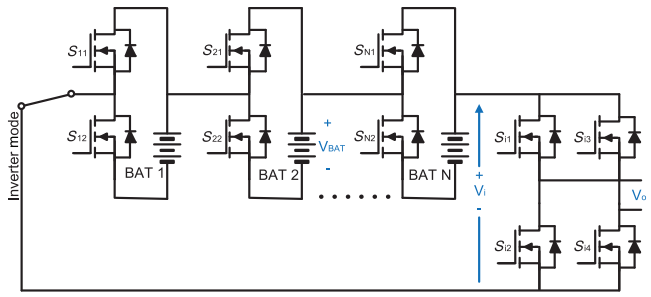

Fig. 5. Equivalent circuit during inverter mode.

inversion mode. As a consequence, only single dc resource is needed. In essence, it shows enhanced functions and high compactness.

TABLE I
SWITCHING STATES OF SWITCHED-BATTERY CIRCUIT DURING INVERTER MODE

V_i	S_{11}	S_{21}	S_{N1}	S_{12}	S_{22}	S_{N2}
0	1	1	1	0	0	0
V_{BAT}	0	1	1	1	0	0
$2V_{BAT}$	0	0	1	1	1	0
NV_{BAT}	0	0	0	1	1	1

Binary logic: 0 = on and 1 = off.

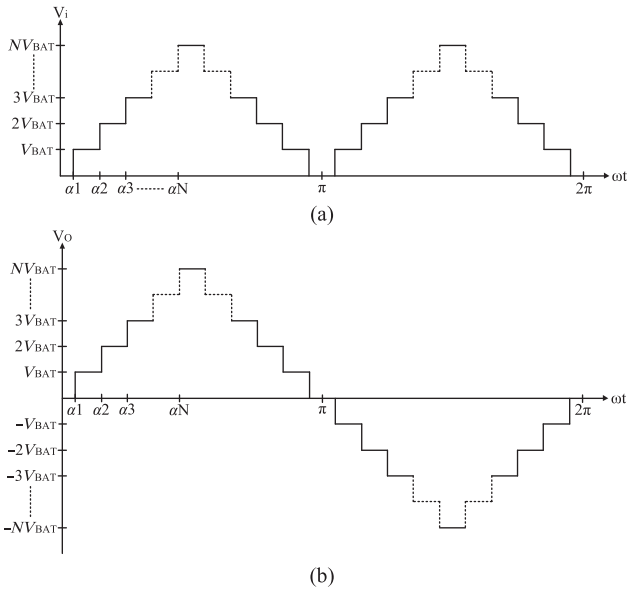

Fig. 6. Inverter key waveforms. (a) Staircase dc-link voltage. (b) Multilevel output ac voltage.

III. SHEPWM WITH GA OPTIMIZATION

A. Inverter Output as a Function of Switching Angles

An important concern in designing an inverter is the power quality of the ac output. The output ac voltage waveform should be sinusoidal-like with low harmonic content. A PWM technique with selective harmonic elimination (SHE) is widely used to control multilevel inverter and produce output voltage with low total harmonic distortion (THD) [24]. Fig. 6(b) shows the

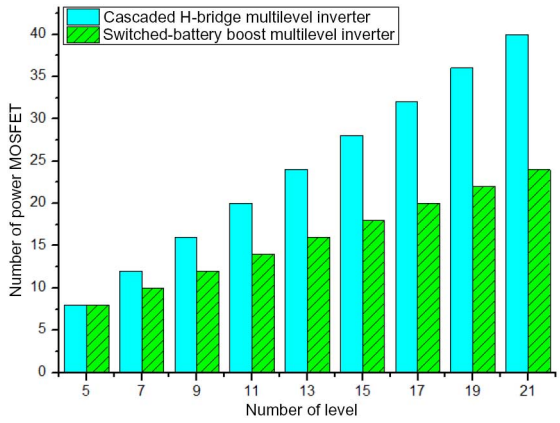

Fig. 7. Comparison of number of power MOSFETs.

output ac voltage of a $2N+1$ level inverter. The multilevel output voltage waveform can be represented mathematically in a Fourier series, as given by

$$v_{\text{out}}(\omega t) = \sum_{h=1,3,5,\ldots}^{\infty} \times \frac{4V_{\text{BAT}}}{h\pi}\left[\cos(h\alpha_1)+\cos(h\alpha_2)+\cdots+\cos(h\alpha_N)\right]\sin(h\omega t). \tag{3}$$

The peak voltage of each h[th] harmonic component is given by

$$V_h = \frac{4V_{\text{BAT}}}{h\pi} \times \left[\cos(h\alpha_1)+\cos(h\alpha_2)+\cdots+\cos(h\alpha_N)\right], \quad h = \text{odd}. \tag{4}$$

The SHE equations can be written by considering the desired fundamental peak voltage, V_1^* and peak voltage of higher order harmonics are zero

$$\begin{aligned} h=1: V_1 &= \frac{4V_{\text{BAT}}}{\pi}\left[\cos(\alpha_1)+\cos(\alpha_2)+\cdots+\cos(\alpha_N)\right] \\ h=3: 0 &= \cos(3\alpha_1)+\cos(3\alpha_2)+\cdots+\cos(3\alpha_N) \\ &\vdots \\ h=2N-1: 0 &= \cos\left[(2N-1)\alpha_1\right] \\ &+\cos\left[(2N-1)\alpha_2\right]+\cdots+\cos\left[(2N-1)\alpha_N\right]. \end{aligned} \tag{5}$$

With N switched-battery cells, the PWM can eliminate up to $2N-1$ harmonic. The modulation index of the inverter is given by

$$M = \frac{\pi V_1}{12V_{\text{BAT}}}, \quad 0 \le M \le 1 \tag{6}$$

where V_1 is the peak of fundamental component.

By combining (1), (5), and (6), the modulation index as a function of number of levels can be written as

$$M = \frac{1}{3}\sum_{i=1,2\ldots}^{(N_{\text{Vo}}-1)/2}\cos(\alpha_i), \quad 0 \le M \le 1 \tag{7}$$

where $0 < \alpha_1 < \alpha_2 < \cdots < \alpha_N < \frac{\pi}{2}$.

B. Genetic Algorithm

The SHE equations in (5) are highly nonlinear, and therefore, difficult to solve. Optimization algorithm can be used to determine the optimum switching angles. Unlike some numerical method, which might not be able to find the solution for certain M [25], optimization algorithm is an intelligent method, which guaranteed existence of solutions throughout the full range of M. Among the various optimization-based techniques introduced in recent decades, two promising algorithm, which have been proven its viability and favorability in SHEPWM problem are GA and particle swarm optimization (PSO) [26]. In recent years, some different optimization algorithms such as bee algorithm (BA) [27] and standard colonial competitive algorithm (CCA) [28] are verified their superiority over GA in terms of better convergence rate. Since this work demands only in acquiring the optimal switching angles and THD minimization regardless of other aspects, GA remains as the preferable option. MATLAB provides a user-friendly way to compute the minimum fitness function using GA. The built-in command ga in MATLAB dedicated to compute constrained and unconstrained optimization problem using GA is as follows:

$$\begin{aligned}&[\alpha, \text{fval}] \\ &= ga(\text{fitnessfcn}, n\,\text{var}\,s, A, b, A\text{eq}, b\text{eq}, \text{LB}, \text{UB}, \text{nonlcon})\end{aligned}$$

where $[\alpha, \text{fval}]$ is the output argument with the fitness function evaluated at α while the nine terms within the bracket imply the input arguments require for the GA computation. Implementation of GA requires a properly defined fitness function (fitnessfcn), number of α in the problem (nvars), linear inequality constraints in the form of $A*\alpha \le b$, linear equality constraints in the form of $A\text{eq}*\alpha = b\text{eq}$, lower bound (LB) and upper bound (UB) of α, and nonlinear constraints (nonlcon).

C. Fitness Function

A suitable fitness function has to be determined to be implemented in the GA algorithm. Distortion of the voltage waveform at fundamental frequency must be mitigated to achieve substantially improved sinusoidal waveform while the higher order harmonics, if made lessen, will further alleviate the THD and lead to a more perfect sine wave. In this instance, the control effort is related to the peak voltage of fundamental V_1 as well as the peak voltage of individual odd harmonic V_h. A proper fitness function is needed to gather the mentioned control variables into a single equation, as mentioned in [29]. However, V_1 is the primary control objective, which deserve more attention than the secondary control objectives V_h. Hence, a weighting factors w is introduced into each odd harmonic to alleviate their influence. The fitness function is expressed as

$$\begin{aligned}\text{Fitness function} &= \left(V_1^* - V_1\right)^2 \\ &+ w_3V_3^2 + w_5V_5^2 + \cdots + w_{2N-1}V_{2N-1}^2\end{aligned} \tag{8}$$

where V_1* is the desired peak of fundamental component according to modulation index in (6), w_h and V_h with $h \in \{3,5,\ldots,2N-1\}$are, respectively, referred to the weighting factor and peak voltage of harmonic associated to each odd

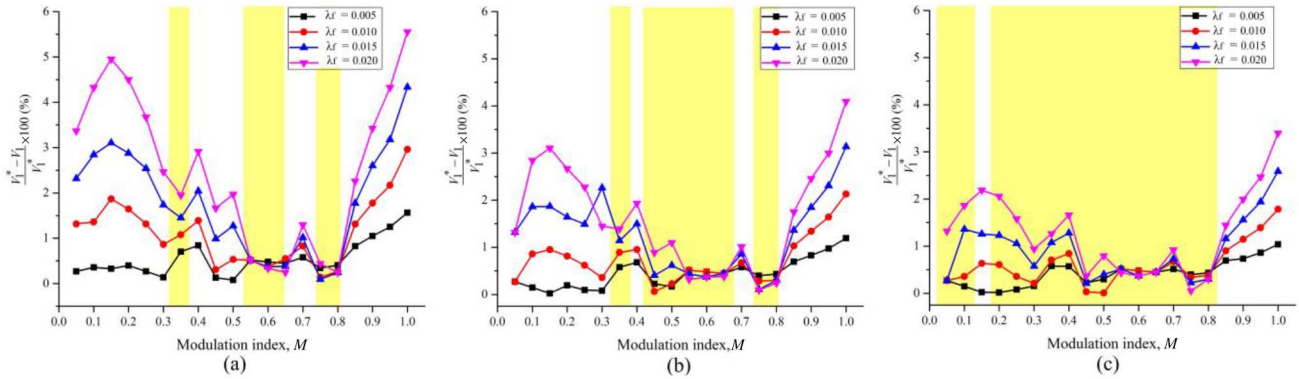

Fig. 8. Primary term control performance for different λ_f and M when (a) $\lambda_h = 0.01$; (b) $\lambda_h = 0.02$; and (c) $\lambda_h = 0.03$.

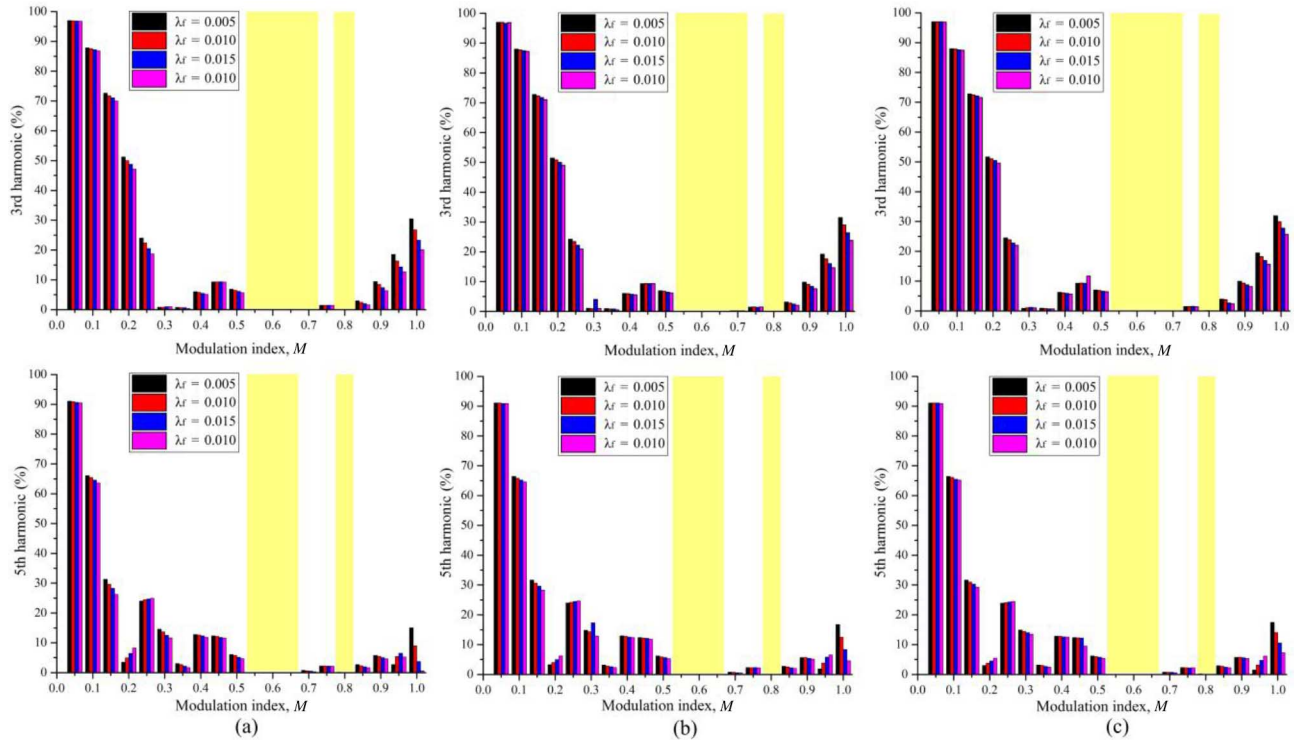

Fig. 9. Secondary terms control performance for different λ_f and M when (a) $\lambda_h = 0.01$; (b) $\lambda_h = 0.02$; and (c) $\lambda_h = 0.03$.

harmonic. Tuning the importance of the respective harmonics is by far remained as an empirical approach, which requires a lot of trial and error efforts [29]. Inappropriate choice of weighting factors can have strong adverse effects on the system. Since practical design requires greater emphasis on lower order harmonics, a direct approach is to weight each harmonic peak voltage by its reciprocal of harmonic order to rule out the necessity for weighting factor adjustment, and thus

$$\text{Fitness function} = (V_1^* - V_1)^2 + \frac{1}{3}V_3^2 + \frac{1}{5}V_5^2 + \cdots + \frac{1}{2N-1}V_{2N-1}^2 \quad (9)$$

which can be written in a more compact form of

$$\text{Fitness function} = (V_1^* - V_1)^2 + \sum_{h=3,5,\ldots}^{2N-1} \frac{1}{h}(V_h)^2 \quad (10)$$

where h is the odd harmonic order of the output voltage. The primary term and secondary term of the fitness function are further normalized considering V_1^* and V_1, respectively, as indicated in

$$V_1^* - V_1 = \lambda_f V_1^*; \quad 0 < \lambda_f \leq 0.02 \quad (11)$$

$$V_h = \lambda_h V_1; \quad 0 < \lambda_h \leq 0.03 \quad (12)$$

where λ_f is the constraint for fundamental harmonic peak voltage with respect to V_1^*, and λ_h is the constraint for each harmonic peak voltage with respect to V_1. The upper bound of λ_f is restricted to as low as 2% in this study. On the other hand, the upper bound of λ_h is also restricted so as to ensure V_h does not exceed V_1 by 3%, as recommended in Standard IEEE-519. The imposed constraints are incorporated into the fitness function, which yields

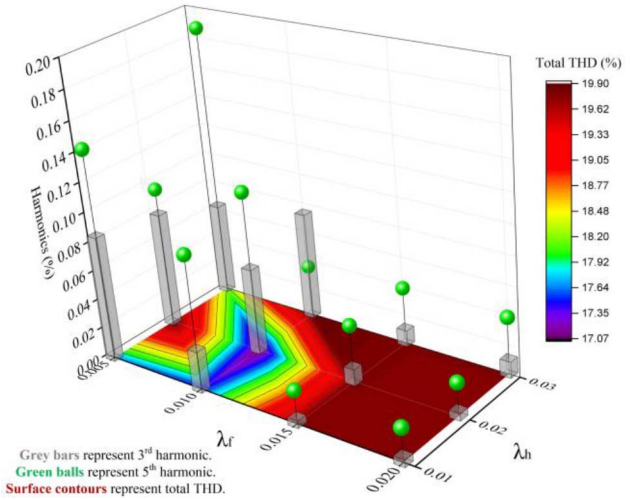

Fig. 10. Determination of λ_f and λ_h with least total THD $(M = 0.8)$.

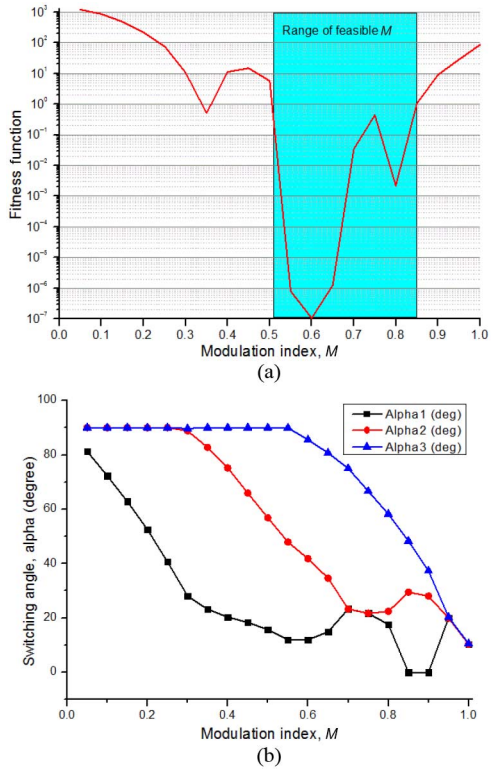

Fig. 11. GA optimization for seven-level switched-battery boost-multilevel inverter. (a) Fitness function. (b) Switching angles.

$$\text{Fitness function} = \left(\frac{1}{\lambda_f}\frac{V_1^* - V_1}{V_1^*}\right)^2 + \sum_{h=3,5,\ldots}^{2N-1} \frac{1}{h}\left(\frac{1}{\lambda_h}\frac{V_h}{V_1}\right)^2. \tag{13}$$

To further to distinguish the primary term from secondary term, any value exceeds the permitted λ_f constraint is subject to a heavy penalty by the power of 4 instead of 2, leading to the final fitness function choice

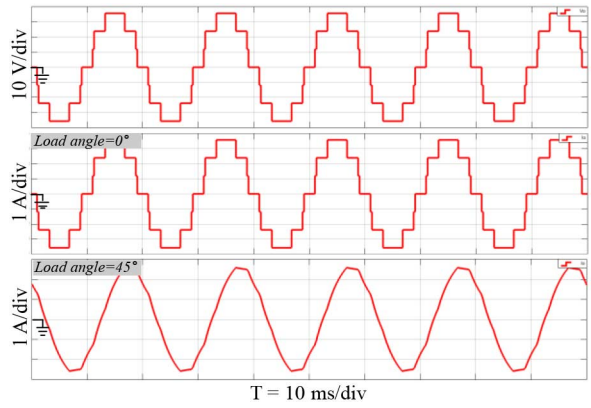

Fig. 12. Simulated output voltage and current waveforms.

$$\text{Fitness function} = \left(\frac{1}{\lambda_f}\frac{V_1^* - V_1}{V_1^*}\right)^4 + \sum_{h=3,5,\ldots}^{2N-1} \frac{1}{h}\left(\frac{1}{\lambda_h}\frac{V_h}{V_1}\right)^2. \tag{14}$$

A parametric study is then carried out to evaluate the performance of the control for different values of λ_f, λ_h, and modulation index. The evaluation is shown in Figs. 8 and 9. The shaded regions in Fig. 8 imply the regions where V_1 satisfy λ_f constraint while the one in Fig. 9 imply the regions where the individual harmonic (third or fifth) satisfy λ_h constraint. An obvious feature obtained from the plots is particularly interesting. Disregard how λ_f or λ_h varies, only certain M fulfills both the imposed constraints of λ_f and λ_h, specifically at region in vicinity of $M = 0.55,\ 0.6,\ 0.65$, and 0.8. The above reasoning implies that only certain M can efficiently eliminates the designated harmonics, which is perfectly consistent with the findings in [27], [28], and [30].

Among the feasible modulation index, region with least total THD is found for $M = 0.8$. Fig. 10 clearly illustrates this region where $\lambda_f = 0.01$ and $\lambda_h = 0.02$. This leads to the finalized fitness function represented in the form

$$\text{Fitness function} = \left(100\frac{V_1^* - V_1}{V_1^*}\right)^4 + \sum_{h=3,5,\ldots}^{2N-1} \frac{1}{h}\left(50\frac{V_h}{V_1}\right)^2 \tag{15}$$

which also found in literatures [27], [28]. The resultant simulation results by using fitness function in (15) are shown in Fig. 11. It can be observed that there is an optimal range of feasible M. In this region, fitness function is extremely low. This indicates that (15) is solved and the calculated switching angles are able to eliminate the desired third and fifth harmonics.

IV. Simulation Results

Simulation using MATLAB Simulink is performed to validate the operating principles of the proposed system. Fig. 12 shows the output voltage and load currents of a seven-level inverter with 12 V batteries. Simulation is conducted for different loads at $M = 0.8$. For purely resistive load $(10\ \Omega)$, the

output current shows staircase like waveform, proportional to the output voltage. Inductive load with load angle of 45° is also simulated with a series connected 31.83 mH inductor. The load current becomes more sinusoidal due to the filtering characteristic of the inductor reactance. In both cases, same output voltage is observed and third and fifth harmonics are eliminated.

The practical power switches used in the experimental prototype were modeled in detail in Simulink to study the switching and conduction power losses of the inverter with GA optimized SHEPWM and conventional sinusoidal PWM. The inverter was simulated under varying load illustrated in Fig. 13. Due to the low switching frequency (100 Hz for switched-battery cells and 50 Hz for full bridge), SHEPWM has assured negligibly small switching power loss in the range of 2–4 mW. The conventional sinusoidal PWM demonstrated much higher switching power loss. As predicted, the conduction power loss of either switching methods increases with power level. It is clearly seen that for all output power, the conduction power loss of sinusoidal PWM is significantly larger than that of SHEPWM due to its higher harmonic contents. The efficiency of the proposed boost-multilevel inverter with GA optimized SHEPWM exceeds 88%.

V. Hardware Implementation

A seven-level inverter prototype shown in Fig. 14 is constructed by using silicon carbide (SiC) power MOSFETs. The storage system uses three 12 V lead acid batteries. An eZdsp F28335 is employed to control the inverter. Two distinctive software packages are required in Simulink and Code Composer Studio (CCS) in programming the DSP controller. Texas Instrument C2000 library supported by Simulink allows direct access to DSP modules such as ePWM, just as in Simulink block. Simulink is configured such that when build is initiated, it generates C codes and automatically launch and linked to CCS to program the DSP controller. Gate driver designed by using optocoupler HCPL3140 play a role in isolating the DSP controller and driving the inverter according to PWM signals. The instantaneous output voltage is displayed on Tektronix TDS2024C digital oscilloscope. The output voltage is stepped down with a ratio of 4:1 by using a potential divider so that the data of output voltage can be logged by using NI USB-6353 data acquisition (DAQ) hardware. LabVIEW is necessary to configure the DAQ hardware of which its sampling rate is set to 100 kHz. LabVIEW also save the logged data in tdms file. This file is read in excel and imported into MATLAB for FFT analysis by using Simulink Powergui block. For experimentation, the switching angles for different modulation index are computed offline and stored in a lookup table.

VI. Experimental Results

For verification, the seven-level inverter was tested for modulation ranges from 0.05 to 1 with step 0.05. The instantaneous output voltage was recorded in both oscilloscope picture and data that logged through DAQ system. THD analysis was performed by using the FFT function of Simulink Powergui. The

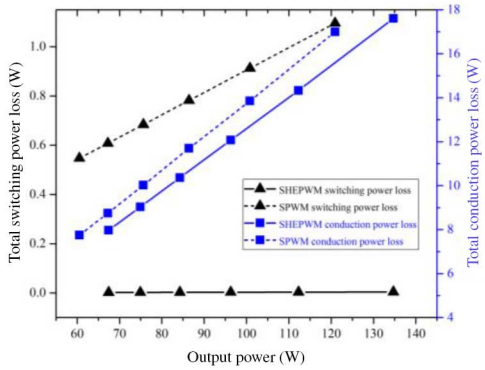

Fig. 13. Comparative study of switching and conduction power losses between SHEPWM and sinusoidal PWM.

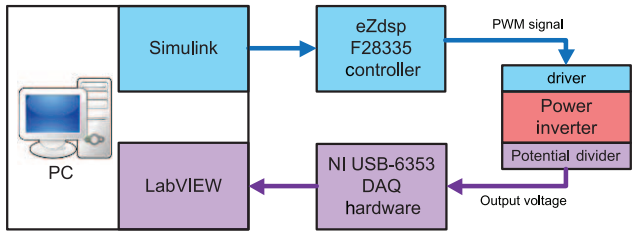

(a)

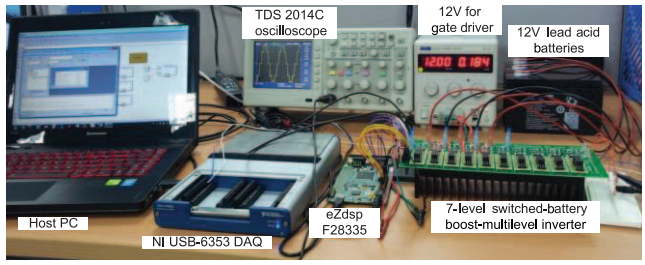

(b)

Fig. 14. Structure of experimental setup.

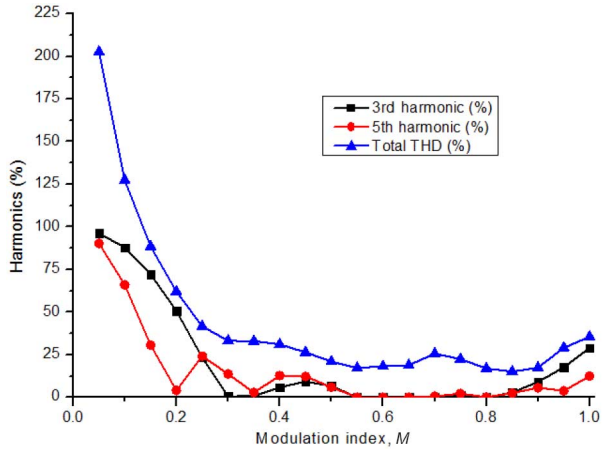

Fig. 15. Percentages of third harmonic, fifth harmonic, and total THD.

analysis results for different modulation index are compared in Fig. 15. The plot shows that the feasible operating point ranges from $M = 0.55$ to $M = 0.85$, during which the third and fifth harmonics are removed effectively, resulting in low total THD within this region. This is also the region where

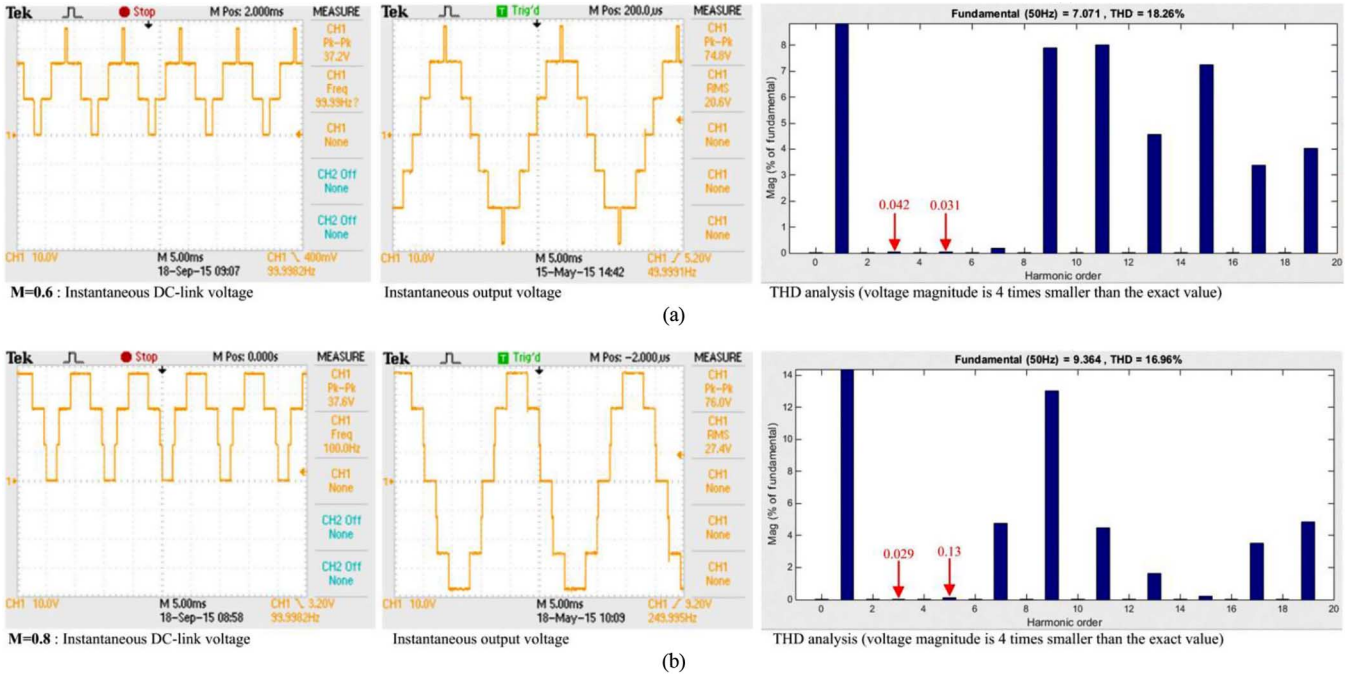

Fig. 16. Voltage waveforms and THD analysis. (a) $M = 0.6$. (b) $M = 0.8$.

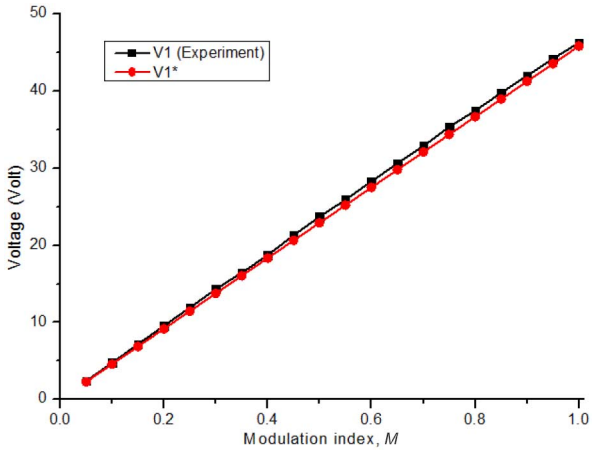

Fig. 17. Comparison of fundamental peak voltage.

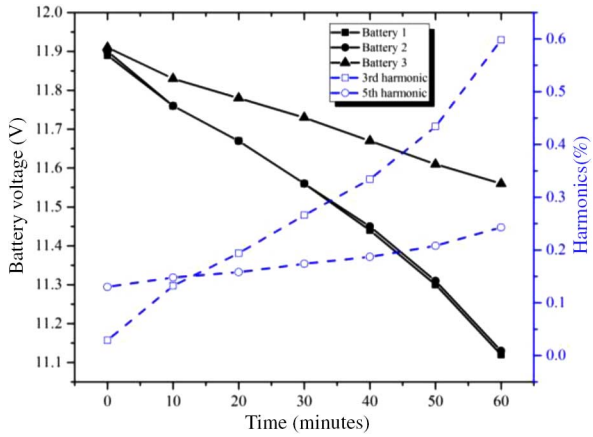

Fig. 18. Batteries voltage for 1 h operation with $M = 0.8$.

low fitness function is found, as discussed in Section III. This feasible operating region is similar with the findings in [27], [28], and [30]. Fig. 16 shows the instantaneous output voltage with THD analysis for $M = 0.6$ and $M = 0.8$. It is clearly seen that the magnitude of third and fifth harmonics are negligible, which proves the feasibility of switched-battery boost-multilevel inverter controlled by SHEPWM. Reduction of higher order harmonics as well as total THD can be done by increasing the number of inverter level, which will significantly increase the voltage boosting ratio as well. As the output voltage is measured with a stepped down ratio of 4:1, the fundamental peak voltage observed in Fig. 16 should be multiplied by 4. The experimental fundamental peak voltage is 28.28 and 37.46 V for $M = 0.6$ and $M = 0.8$, respectively, which is compatible with the theoretical computations from (6). Fig. 17 illustrates the comparison of fundamental peak voltage between the calculated reference theoretical value and the experimental results. Both curves are very close to each other, illustrating that the experimental results are in good agreement with theoretical values.

The inverter controlled by SHEPWM with $M = 0.8$ was tested under 10 Ω resistor. Fig. 18 shows the batteries discharge at uneven rates, due to the fact that the discharging period of each battery is switching angle dependent. For $M = 0.8$, α_1, α_2, and α_3 are 17.64°, 22.43°, and 58.23° respectively. The conduction period for batteries 1 and 2 differ only 4.8° and hence result in similar voltage. However, battery 3 discharges slowly due to its much shorter discharging period (larger switching angle). Voltage unbalance owing to different discharging period of batteries causes the increment of third and fifth harmonics as illustrated in Fig. 18. This, however, is not a major concern as that the thirdand fifth harmonics are both less than 3% and still meet the requirements in Standard IEEE-519.

Conventional sinusoidal PWM switching technique was also implemented with the hardware topology to produce 26.2 V

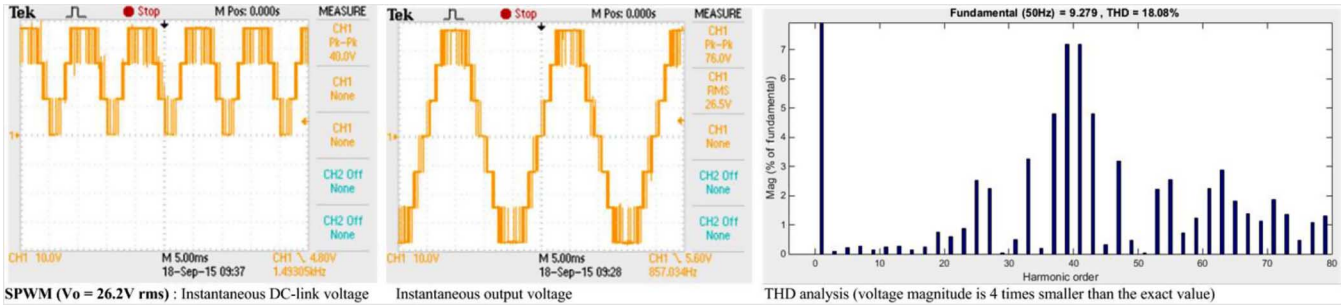

Fig. 19. Voltage waveforms and THD analysis of inverter controlled by sinusoidal PWM.

(rms); approximately the voltage of SHEPWM at $M = 0.8$ in Fig. 16(b). Fig. 19 shows the instantaneous voltage waveforms and THD analysis for 2 kHz switching frequency. This switching technique has larger total THD of 18.08%, compared to 16.96% for GA optimized SHEPWM. In addition, the sinusoidal PWM requires higher switching frequency, which results in higher switching loss. This clearly demonstrates the advantages of our proposed design.

VII. Conclusion

In this paper, the working concept of a switched-battery boost-multilevel inverter was discussed and verified by both numerical simulations and experimental tests. The multifunctional inverter is capable of operating in either battery charging mode or inverter mode, which makes it particularly suitable for standalone application such as PV system. In addition, it requires much less power switches and only single dc resource, which is particularly attractive in practical applications. GA algorithm is used to optimize the switching angles for selectively eliminating voltage harmonics as specified in the fitness function. The optimization also performed such that the fundamental voltage component can be controlled according to the modulation index M. A seven-level inverter system has been implemented for experimentation and the results show that the feasible operating point ranges from $M = 0.55$ to $M = 0.8$ where the third and fifth harmonics are removed effectively. The experimental results show good agreement with theoretical concept and have proven the feasibility of the inverter system. In the experiment, it was observed that as the batteries discharged, the third and fifth harmonics increased due to the unbalanced discharging. Although it was not a problem in the experiment as the harmonic components still satisfied the requirement, it can be expected that as the batteries continue to discharge, the harmonic components will eventually violate the performance constraints. To address this problem, a systematic power management and control design algorithm will need to be developed. This forms part of our future research and will be reported separately.

References

[1] J. M. Guerrero, L. J. Hang, and J. Uceda, "Control of distributed uninterruptible power supply systems," *IEEE Trans. Ind. Electron.*, vol. 55, no. 8, pp. 2845–2859, Aug. 2008.

[2] F. Blaabjerg, Y. Yang, and K. Ma, "Power electronics - key technology for renewable energy systems - Status and future," in *Proc. 3rd Int. Conf. Elect. Power Energy Convers. Syst. (EPECS'13)*, 2013, pp. 1–6.

[3] H. Borhanazad, S. Mekhilef, R. Saidur, and G. Boroumandjazi, "Potential application of renewable energy for rural electrification in Malaysia," *Renew. Energy*, vol. 59, pp. 210–219, 2013.

[4] E. Ribeiro, A. J. M. Cardoso, and C. Boccaletti, "Modular hybrid storage system for renewable energy standalone power supplies," in *Proc. 39th Annu. Conf. IEEE Ind. Electron. Soc.*, 2013, pp. 1749–1754.

[5] F. L. Luo and H. Ye, *Advanced DC/AC Inverters: Applications in Renewable Energy*, 1st ed. Boca Raton, FL, USA: CRC Press, 2013.

[6] C. Cecati, F. Ciancetta, and P. Siano, "A multilevel inverter for photovoltaic systems with fuzzy logic control," *IEEE Trans. Ind. Electron.*, vol. 57, no. 12, pp. 4115–4125, Dec. 2010.

[7] J. S. Lai and F. Z. Peng, "Multilevel converters-a new breed of power converters," *IEEE Trans. Ind. Appl.*, vol. 32, no. 3, pp. 509–517, May/Jun. 1996.

[8] J. Rodríguez, J.-S. Lai, and Z. P. Fang, "Multilevel inverters: A survey of topologies, controls, and applications," *IEEE Trans. Ind. Electron.*, vol. 49, no. 4, pp. 724–738, Aug. 2002.

[9] M. H. Rashid, *Power Electronics: Circuits, Devices and Applications*, 3rd ed. Englewood Cliffs, NJ, USA: Prentice-Hall, 2003.

[10] R. M. Nakagomi, Y. Zhao, and B. Lehman, "Multi-level converters for three-phase photovoltaic applications," in *Proc. 12th IEEE Workshop Control Model. Power Electron.*, 2010, pp. 1–6.

[11] S. Busquets-Monge, J. Rocabert, P. Rodríguez, S. Alepuz, and J. Bordonau, "Multilevel diode-clamped converter for photovoltaic generators with independent voltage control of each solar array," *IEEE Trans. Ind. Electron.*, vol. 55, no. 7, pp. 2713–2723, Jul. 2008.

[12] E. Ozdemir, S. Ozdemir, and L. M. Tolbert, "Fundamental-frequency-modulated six-level diode-clamped multilevel inverter for three-phase stand-alone photovoltaic system," *IEEE Trans. Ind. Electron.*, vol. 56, no. 11, pp. 4407–4415, Nov. 2009.

[13] H. Patangia and D. Gregory, "An efficient cascaded multilevel inverter suited for PV application," in *Proc. 35th IEEE Photovoltaic Spec. Conf. (PVSC'10)*, 2010, pp. 2859–2863.

[14] Y. Zhou and H. Li, "Analysis and suppression of leakage current in cascaded-multilevel-inverter-based PV systems," *IEEE Trans. Power Electron.*, vol. 29, no. 10, pp. 5265–5277, Oct. 2014.

[15] S. A. Khajehoddin, P. Jain, and A. Bakhshai, "Cascaded multilevel converters and their applications in photovoltaic systems," in *Proc. 2nd Can. Solar Build. Conf.*, 2007, pp. 2–7.

[16] M. I. Desconzi, R. C. Beltrame, C. Rech, L. Schuch, and H. L. Hey, "Photovoltaic stand-alone power generation system with multilevel inverter key words," in *Proc. Int. Conf. Renew. Energ. Power Quality*, 2010, pp. 1–6.

[17] M. Sadikin, T. Senjyu, and A. Yona, "High-frequency link DC for power quality improvement of stand-alone PV system in cascaded multilevel inverter," in *Proc. IEEE 10th Int. Conf. Power Electron. Drive Syst.*, 2013, pp. 597–601.

[18] A. Chitra and S. Himavathi, "System for cascade H-bridge multilevel inverter," in *Proc. 2013Int. Conf. Power Energy Control*, 2013, pp. 260–265.

[19] Sé. Daher, Jü. Schmid, and F. L. M. Antunes, "Multilevel inverter topologies for stand-alone PV systems," *IEEE Trans. Ind. Electron.*, vol. 55, no. 7, pp. 2703–2712, Jul. 2008.

[20] F.-S. Kang, S.-J. Park, S. E. Cho, C.-U. Kim, and T. Ise, "Multilevel PWM inverters suitable for the use of stand-alone photovoltaic power systems," *Energy*, vol. 20, no. 4, pp. 906–915, 2005.

[21] K. Gupta, A. Ranjan, P. Bhatnagar, L. K. Sahu, and S. Jain, "Multilevel inverter topologies with reduced device count: A review," *IEEE Trans. Power Electron.*, vol. 31, no. 1, pp. 131–151, Jan. 2016.
[22] A. Rout, S. Samantara, G. K. Dash, S. Choudhury, R. Sharma, and B. Dash, "Modeling and simulation of hybrid MPPT based standalone PV system with upgraded multilevel inverter," in *Proc. 2014 Annu. IEEE India Conf. (INDICON'14)*, 2014, pp. 1–6.
[23] G.-J. Su, "Multilevel DC-link inverter," *IEEE Trans. Ind. Appl.*, vol. 41, no. 3, pp. 848–854, May/Jun. 2005.
[24] C. Buccella, C. Cecati, M. G. Cimoroni, and K. Razi, "Analytical method for pattern generation in five-level cascaded H-bridge inverter using selective harmonic elimination," *IEEE Trans. Ind. Electron.*, vol. 61, no. 11, pp. 5811–5819, Nov. 2014.
[25] K. Yang, Z. Yuan, R. Yuan, W. Yu, J. Yuan, and J. Wang, "A groebner bases theory based method for selective harmonic elimination," *IEEE Trans. Power Electron.*, vol. 30, no. 12, pp. 6581–6592, Dec. 2015.
[26] M. S. A. Dahidah, G. Konstantinou, and V. G. Agelidis, "A review of multilevel selective harmonic elimination PWM : Formulations, solving algorithms, implementation and applications," *IEEE Trans. Power Electron.*, vol. 30, no. 8, pp. 4091–4106, Aug. 2015.
[27] A. Kavousi, B. Vahidi, R. Salehi, M. K. Bakhshizadeh, N. Farokhnia, and S. H. Fathi, "Application of the bee algorithm for selective harmonic elimination strategy in multilevel inverters," *IEEE Trans. Power Electron.*, vol. 27, no. 4, pp. 1689–1696, Apr. 2012.
[28] M. H. Etesami, N. Farokhnia, and S. H. Fathi, "Colonial competitive algorithm development toward harmonic minimization in multilevel inverters," *IEEE Trans. Ind. Informat.*, vol. 11, no. 2, pp. 459–466, Apr. 2015.
[29] P. Cortes *et al.*, "Guidelines for weighting factors design in model predictive control of power converters and drives," in *Proc. IEEE Int. Conf. Ind. Technol.*, 2009, pp. 1–7.
[30] V. Roberge, M. Tarbouchi, and F. Okou, "Strategies to accelerate harmonic minimization in multilevel inverters using a parallel genetic algorithm on graphical processing unit," *IEEE Trans. Power Electron.*, vol. 29, no. 10, pp. 5087–5090, Oct. 2014.

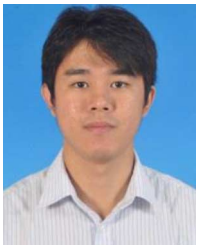

Sze Sing Lee (M'14) received the B.Eng. (Hons.) and Ph.D. degrees in electrical engineering from the University of Science Malaysia, Penang, Malaysia, in 2010 and 2013, respectively.

In August 2013, he was appointed as a Senior Lecturer with the School of Electrical Systems Engineering, Universiti Malaysia Perlis, Malaysia. He is currently with the University of Southampton Malaysia Campus (USMC), Johor Bahru, Malaysia. His research interests include alternative power converter topologies and control strategies for renewable energy integration.

Bing Chu received the B.Eng. degree in automation and the M.Sc. degree in control science and technology from Tsinghua University, Beijing, China, and the Ph.D. degree in automatic control and systems engineering from The University of Sheffield, Sheffield, U.K., in 2004, 2007, and 2009, respectively.

He is a Lecturer of Electronics and Computer Science with the University of Southampton, Southampton, U.K. Before joining the University of Southampton in 2012, he was a Postdoctoral Researcher with the University of Oxford, Oxford, U.K. (2010–2012). His research interests include iterative learning and repetitive control, analysis and control of large-scale networked systems, applied optimization theory, and their applications to robotics, power electronics, and next-generation healthcare.

Dr. Chu was the recipient of a number of awards including the Best Paper Prize of the 2012 United Kingdom Automatic Control Council International Conference on Control and the Certificate of Merit for the 2010 IET Control and Automation Doctoral Dissertation Prize.

Nik Rumzi Nik Idris (SM'03) received the B.Eng. degree in electrical engineering from the University of Wollongong, Wollongong, Australia, the M.Sc. degree in power electronics from Bradford University, Bradford, U.K., and the Ph.D. degree from the Universiti Teknologi Malaysia (UTM), Johor, Malaysia, in 1989, 1993, and 2000, respectively.

He is an Associate Professor with the Universiti Teknologi Malaysia, and currently the Chair for the Power Electronics Chapter of the IEEE Malaysia Section. His research interests include control of ac drive systems and DSP applications in power electronic systems.

Hui Hwang Goh (SM'12) received the B.Eng. degree in electrical engineering, the M.Eng. degree in electrical engineering, and the Ph.D. degree from the Universiti Teknologi Malaysia (UTM), Johor, Malaysia, in 1998, 2002, and 2007, respectively.

He is currently an Associate Professor with the Department of Electrical Power Engineering, Faculty of Electrical and Electronic Engineering, Universiti Tun Hussein Onn Malaysia, Parit Raja, Malaysia. His research interests include embedded power generation modeling and simulation, power quality studies, wavelet analysis, multicriteria decision making, renewable energies, and dynamic equivalent.

Dr. Goh is a member of the Institution of Engineering and Technology, U.K. He is also a member of the Institution of Engineers, Malaysia (IEM), a Chartered Engineer under the Engineering Council United Kingdom (ECUK), and a Professional Engineer under the Board of Engineers, Malaysia (BEM).

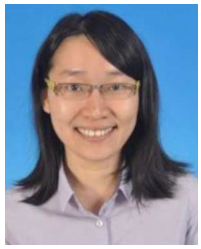

Yeh En Heng received the B.Eng. (Hons.) and M.Sc. degrees in electronics engineering from the University of Science Malaysia, Penang, Malaysia, in 2010 and 2014, respectively.

She is currently a Research Assistant with the University of Southampton Malaysia Campus (USMC), Johor Bahru, Malaysia. Her research interests include advanced control techniques using predictive control theory and computational intelligence for power inverter systems.